SCIENTIFIC REPORTS

OPEN

SUBJECT AREAS:
TRANSMISSION ELECTRON MICROSCOPY
MAGNETIC PROPERTIES AND MATERIALS
INFORMATION STORAGE
CHARACTERIZATION AND ANALYTICAL TECHNIQUES

Received
25 April 2013

Accepted
23 July 2013

Published
12 August 2013

Correspondence and requests for materials should be addressed to A.K. (akohn@exchange.bgu.ac.il)

The antiferromagnetic structures of $IrMn_3$ and their influence on exchange-bias

A. Kohn[1,2], A. Kovács[3], R. Fan[4], G. J. McIntyre[5], R. C. C. Ward[6] & J. P. Goff[7]

[1]Department of Materials Engineering, Ben-Gurion University of the Negev, Beer-Sheva 84105, Israel, [2]Ilse Katz Institute for Nanoscale Science and Technology, Ben-Gurion University of the Negev, Beer-Sheva 84105, Israel, [3]Ernst Ruska-Centre for Microscopy and Spectroscopy with Electrons, Peter Grünberg Institute, Forschungszentrum Jülich, Jülich 52425, Germany, [4]Diamond Light Source, Harwell Science and Innovation Campus, Didcot OX11 0DE, United Kingdom, [5]Australian Nuclear Science and Technology Organisation, Lucas Heights, New South Wales 2234, Australia, [6]Clarendon Laboratory, Department of Physics, University of Oxford, Oxford OX1 3PU, United Kingdom, [7]Department of Physics, Royal Holloway, University of London, Egham, Surrey TW20 0EX, United Kingdom.

We have determined the magnetic structures of single-crystal thin-films of $IrMn_3$ for the crystallographic phases of chemically-ordered $L1_2$, and for chemically-disordered face-centred-cubic, which is the phase typically chosen for information-storage devices. For the chemically-ordered $L1_2$ thin-film, we find the same triangular magnetic structure as reported for the bulk material. We determine the magnetic structure of the chemically-disordered face-centred-cubic alloy for the first time, which differs from theoretical predictions, with magnetic moments tilted away from the crystal diagonals towards the face-planes. We study the influence of these two antiferromagnetic structures on the exchange-bias properties of an epitaxial body-centred-cubic Fe layer showing that magnetization reversal mechanism and bias-field in the ferromagnetic layer is altered significantly. We report a change of reversal mechanism from in-plane nucleation of 90° domain-walls when coupled to the newly reported cubic structure towards a rotational process, including an out-of-plane magnetization component when coupled to the $L1_2$ triangular structure.

'Exchange-bias' occurs when a ferromagnetic layer is coupled to an antiferromagnetic layer thus introducing unidirectional anisotropy due to interface coupling. This anisotropy typically manifests itself by a horizontal offset of the magnetization hysteresis curve, which is quantified by an exchange-bias field, H_{EB}, as well as an increased coercivity field, H_C[1–5]. The exchange-bias phenomenon is of technological importance for information-storage devices, for example to pin the magnetization of the reference magnetic layer in a magnetic tunnel junction or to stabilize magnetic moments in nanoparticles against thermal excitations[6]. As an interface effect, exchange-bias is sensitive to structural parameters that can affect significantly magnetic coupling, such as roughness[7] and chemical-intermixing[8]. The structure of the antiferromagnetic layer, which in technological applications is usually polycrystalline, is also important, for example the degree of preferred crystallographic orientation and the presence and fractional volume of grain boundaries.

These structural parameters result in a rich physical phenomenon, for which quantitative understanding is a subject of ongoing research. Consequently, differentiating and understanding the contribution of the antiferromagnetic structure to unidirectional-anisotropy is challenging[2–5,9].

We examine the influence of the antiferromagnetic structure to exchange-bias in the case of $IrMn_3$, which has two crystallographic phases, γ-$IrMn_3$ and $L1_2$-$IrMn_3$. γ-$IrMn_3$ is face-centered-cubic (FCC, space group 225, lattice parameter, a = 0.378 nm) in which Ir and Mn atoms do not have specific lattice-site preferences. Thermal annealing above 700 K can induce Cu_3Au-type atomic-ordering ($L1_2$, space group 221, a = 0.3772 nm), with negligible change of lattice parameter, where Mn atoms occupy face-central sites. The Néel temperature of $IrMn_3$ is high, around 730 K and 1000 K for γ- and $L1_2$- phases, respectively[10]. Chemically disordered Ir_xMn_{1-x} ($0.15<x<0.25$) alloys are of technological importance, used widely in information-storage devices due to a large exchange-bias field and thermal stability[11].

For chemically-disordered γ-$IrMn_3$, the magnetic structure is of cubic symmetry, though the alignment of magnetic moments *has not been resolved experimentally*. Based on neutron diffraction studies, Yamaoka *et al.* suggest for bulk γ-$IrMn_3$ the so-called 3Q (body diagonal, <111> directions) and 1Q cubic-type structures (<100> directions) as possible solutions, with preference for 1Q[12]. First-principles calculations of Sakuma *et al.* suggest that 3Q is energetically preferable for γ-$IrMn_3$ followed by 2Q (<110> directions), and finally 1Q, assuming bulk lattice-parameters without strain[13].

The magnetic structure of bulk $L1_2$-$IrMn_3$, which was determined by neutron scattering experiments[14], and by theoretical calculations[13], is the so-called triangular, T1, structure in which Mn moments are parallel to {111} planes and aligned in <112> directions (Fig. 1a). Calculations[13] show that exchange-interactions acting on Mn magnetic moments in $L1_2$-$IrMn_3$ are significantly stronger than in γ-$IrMn_3$, as manifested by a higher Néel temperature. Szunyogh *et al.*[15] predict giant second-order magnetic anisotropy for ordered $L1_2$-$IrMn_3$, and consequently, a large increase of the exchange-bias field with respect to a ferromagnet coupled to γ-$IrMn_3$.

Experimentally, enhanced exchange-bias fields of polycrystalline Co-Fe thin films coupled to polycrystalline $L1_2$-$IrMn_3$ films (ordering parameter above 0.5) with {111} crystallographic texture was indeed reported with interfacial exchange-energy coupling, J_K, optimized to exceed 1 erg/cm^2 [16].

Szunyogh *et al.*[17] calculated magnetic anisotropy and exchange interactions at the $L1_2$-$IrMn_3$/FCC-Co(111) interface. The authors report that these two properties are influenced in the immediate vicinity of the interface. Exchange-interactions between Mn and Co atoms are weak, meaning that the bulk magnetic structures are not affected strongly even at the interface. However, symmetry breaking at the interface results in large anisotropy effects causing perpendicular coupling of Co and Mn moments and in unidirectional exchange-anisotropy, which is expected to influence substantially exchange-bias in such systems.

In this work, γ- and $L1_2$-$IrMn_3$ epitaxial thin films, exchange-coupled to an epitaxial body-centered cubic (BCC) Fe film, were grown by molecular beam epitaxy (MBE). We show that the structure of these two types of bilayers is well-defined, namely single-crystal (001) orientation throughout the layer stack, fixed in-plane epitaxial relations, and sharp interfaces with minimal roughness or intermixing. Thus, the MBE growth technique has achieved highly similar interfaces between BCC-Fe and chemically ordered- or disordered-$IrMn_3$.

This structural quality and especially the structural similarity of the exchange-biased bilayers at the atomic-scale were demonstrated by aberration-corrected transmission electron microscopy (TEM) and X-ray diffraction (XRD) measurements.

The magnetic structure of these $IrMn_3$ films was investigated by single-crystal neutron diffraction. For chemically-ordered $L1_2$-$IrMn_3$ films, we confirm the T1 structure reported for bulk crystals. For chemically-disordered γ-$IrMn_3$ films, we have determined experimentally the antiferromagnetic structure for the first time. In contrast to predictions for bulk γ-$IrMn_3$ crystals, we find *a new spin density wave phase* in the thin films in which magnetic moments are tilted away by 45° from crystal diagonals towards the cube faces (Fig. 1b).

Consequently, and in light of theoretical predictions[15,17], we studied the influence of these two $IrMn_3$ antiferromagnetic structures on interface-coupling to an epitaxial ferromagnetic Fe layer, showing a significant change in both the reversal mechanism of magnetic moments in the Fe layer and the magnitude of the exchange-bias field.

Results

Structure of the exchange-biased bilayers: γ-$IrMn_3$ and $L1_2$-$IrMn_3$. The chemically-disordered γ-$IrMn_3$ layer was grown in the following sequence on MgO(001) substrates: MgO/Fe(7 nm)/γ-$IrMn_3$(15 nm)/Cr. The ordered $L1_2$-$IrMn_3$ layer was achieved by growing on an Ir seed layer: MgO/Ir/$L1_2$-$IrMn_3$(15 nm)/Fe(7 nm)/Cr. These multilayer structures are shown in cross-sectional chemical-maps calculated from energy-filtered TEM images (Fig. 2a,b).

We note that chemical ordering of the $IrMn_3$ layer was not achieved when deposited onto Fe. Increasing the growth temperature to 400 °C or post-deposition annealing up to 500 °C did not induce atomic ordering either. *Ex situ* XRD measurements of chemically-disordered $IrMn_3$ in the bilayers measured an out-of-plane lattice parameter of 0.3736 ± 0.0008 nm with less than 2° in-plane mosaic

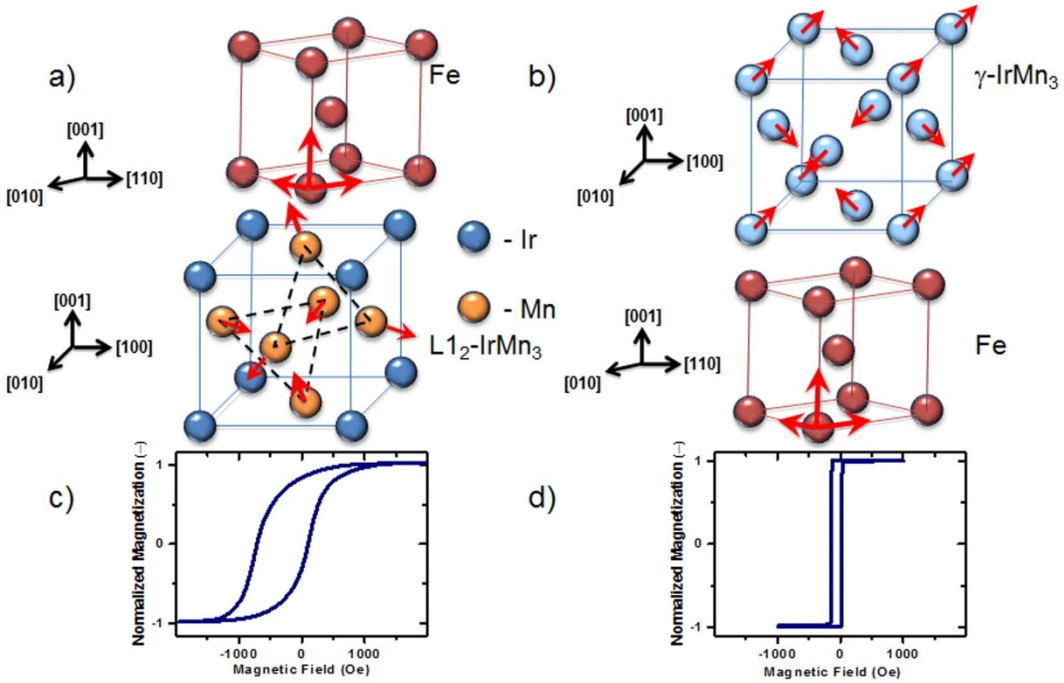

Figure 1 | Schematic representation of crystallographic and magnetic structures of epitaxial bcc-Fe and $IrMn_3$ thin films, which determine the unidirectional anisotropy and hence the reversal mechanism of magnetic moments in the exchange-biased Fe layer. Magnetic structures characterized in this research: T1, chemically-ordered $L1_2$-$IrMn_3$(a), and a newly characterized spin-density wave structure of chemically-disordered γ-$IrMn_3$(b). The significant influence of $IrMn_3$ antiferromagnetic structure on interface-coupling of the epitaxial Fe layer as manifested by magnetization hysteresis loops of Fe exchange-biased to $L1_2$-$IrMn_3$(c) and γ-$IrMn_3$(d) (magnetic field applied along Fe[100] unidirectional axis).

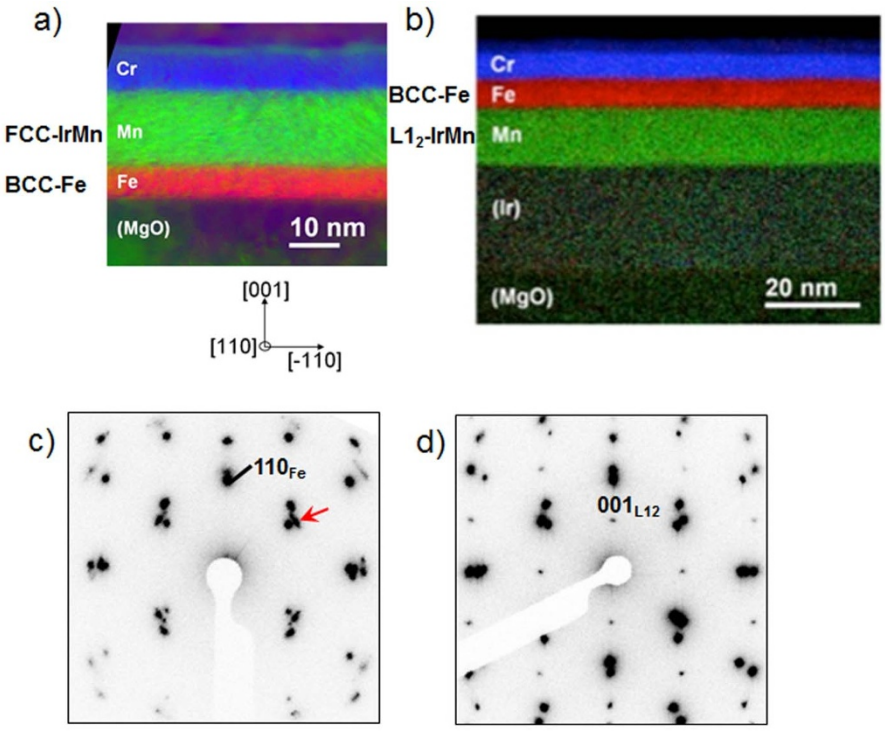

Figure 2 | Structure of exchange-biased layers. Cross-sectional low-loss (left, a) and core-loss (right, b) energy-filtered TEM chemical-mapping reveals sharp interfaces between Fe(red) and γ-$IrMn_3$(green)(a) and between $L1_2$-$IrMn_3$(green) and Fe(red) layers(b). SAED patterns show γ- (c) and $L1_2$-structure (d) of the $IrMn_3$ layer. The red arrow indicates in-plane misorientation of γ-$IrMn_3$ grains.

spread. The in-plane lattice constant, 0.380 nm, is slightly larger than the bulk value, which suggests that the film is expansively strained in-plane by the MgO substrate due to incomplete relaxation of lattice-mismatch strain or substrate clamping during cooling from the growth or anneal temperature.

Growth of $IrMn_3$ on an Ir seed layer at 400 °C does result in the $L1_2$-structure with a chemical-ordering parameter above 0.86 (see methodology section for definition), and an out-of-plane lattice parameter of 0.3725 ± 0.0005 nm. The mosaic spread of this layer is similar to γ-$IrMn_3$, approximately 2°. Measurements of the off-axis Fe(202) reflection detect minor tetragonal distortion in the Fe layer. Here too, the in-plane lattice constant of $L1_2$-$IrMn_3$ is 0.381 nm, again attributed to epitaxial tensile strain.

Cross-sectional chemical-maps (Fig. 2a,b) reveal sharp compositional interfaces between the Fe and $IrMn_3$ layers. Selected area electron diffraction (SAED) patterns (Fig. 2c,d) determine the following epitaxial relation between the layers, regardless of the $IrMn_3$ crystallographic phase: (001)[110]$IrMn_3$||(001)[100]Fe, depicted schematically in Fig. 1. The lack of, and appearance of {010} and {110} reflections in γ-$IrMn_3$ and $L1_2$-$IrMn_3$ SAED patterns, respectively (Fig. 2c,d), confirm their respective crystallographic structures.

The structure of the interfaces was studied by high-resolution (phase contrast) aberration-adjusted TEM (HRTEM) images, shown in Fig. 3a,b for FCC and $L1_2$-$IrMn_3$ layers, respectively. Analyses of these interfaces reveal atomic-column steps and misfit dislocations due to strain relaxation, namely semi-coherent interfaces. Multislice HRTEM image-simulations of interfaces using γ-, $L1_2$-$IrMn_3$ and Fe structures are embedded in Fig. 3a,b, respectively. In the γ-$IrMn_3$ phase, Ir and Mn atoms occupy randomly FCC atomic-sites, while in the $L1_2$-structure, planes of Mn atoms and mixed Ir and Mn atoms alternate along the [001] direction, which results in periodic variations of image intensity for atomic planes observed along the [001] direction (Fig. 3b). Atomic layers with the largest measured image intensity correspond to those containing both Ir and Mn atoms. Fig. 3c shows an aberration-corrected high-resolution scanning

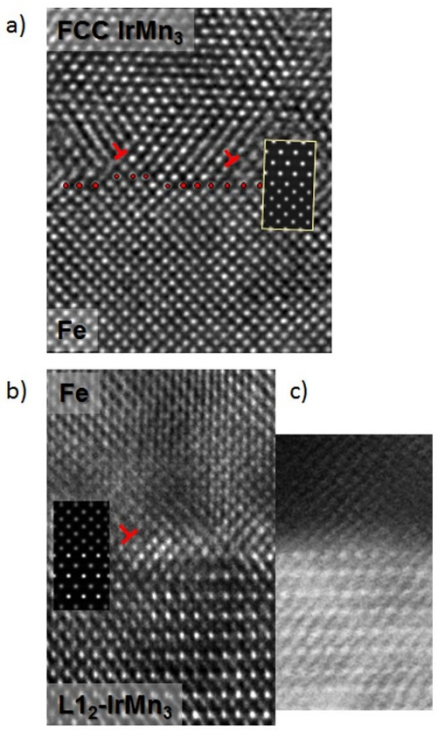

Figure 3 | Interface structure of $IrMn_3$ and Fe layers characterized by HRTEM. Surface steps and misfit dislocations (highlighted with red markers) decorate both γ-$IrMn_3$/Fe interfaces(a) and Fe/$L1_2$-$IrMn_3$ interfaces(b,c-HAADF-STEM image). For this region, the terminating layer in this $L1_2$-$IrMn_3$ antiferromagnet is the Ir-Mn plane. Multislice simulations of interfaces are embedded in the HRTEM images.

TEM (STEM) image recorded with a high-angle annular dark-field (HAADF) detector from the same region. In this imaging mode, the intensity of atomic-columns is proportional to the atomic number confirming the presence of heavy Ir atoms at the interface. For the example region shown here, these imaging modes indicate that the terminating layer in the $L1_2$-$IrMn_3$ layer is the Ir-Mn plane. We observed consistently that the interfaces are chemically sharp, though we did not control the terminating layer, which may alternate between Ir-Mn and Mn within the same sample.

Overall, we demonstrate high structural quality of the two types of exchange-biased epitaxial bilayers, in particular sharp interfaces and negligible chemical intermixing, as well as similarity of the two bilayers in terms of composition and crystallographic epitaxial relations and lattice parameters.

Therefore, we proceed to characterize the magnetic structure of the two types of $IrMn_3$ thin films.

Magnetic structure of γ- and $L1_2$- $IrMn_3$ epitaxial films. The magnetic structure of $IrMn_3$ was investigated by neutron diffraction experiments on 200 nm thick films. Fig. 4a shows the observed magnetic structure factors for all accessible reflections in chemically-disordered γ-$IrMn_3$. Structural scattering is not observed because, for the $IrMn_3$ composition, the contribution of the two nuclear scattering lengths approximately cancel. The calculated magnetic structure factors (blue points) are the best fit to the observed intensity using the model (Fig. 4b inset, $\theta = \phi = 45^\circ$) proposed for antiferromagnetic disordered γ-Fe-Mn alloys[18]. Fig. 4b plots the χ^2 goodness of fit test as a function of inter-spin angle, θ, defined in the inset. We find that $\theta = 45^\circ \pm 2^\circ$, which indicates clearly towards a *new magnetic structure* of γ-$IrMn_3$ and rules out the 1Q, 2Q or 3Q structures proposed for bulk γ-$IrMn_3$. This new magnetic structure is characterized by cubic-symmetry in which moments are tilted away by 45° from crystal-face diagonals towards the cube faces.

Using a similar neutron scattering approach, the magnetic structure of chemically-ordered $L1_2$-$IrMn_3$ film was characterized. Fig. 4c shows the observed magnetic structure factors compared to calculated values according to the structure shown in Fig. 1a. These results are consistent with the T1-structure of bulk $L1_2$-$IrMn_3$ reported previously[14].

We have thus characterized the different magnetic structures of the two $IrMn_3$ crystallographic phases. These results and the previous structural characterization now enable to examine specifically the influence of the antiferromagnetic structure of $IrMn_3$ on interface-coupling of the epitaxial Fe layer through exchange-bias.

Magnetic properties. We examined magnetization reversal of Fe moments coupled to antiferromagnetic γ-$IrMn_3$ by vibrating sample magnetometry. Fig. 5 shows hysteresis loops of magnetization, M, as a function of applied field, H, directed in-plane along the Fe[100] easy-axis and magnetic annealing direction (a), Fe[110] minor hard-axis direction (b), and Fe[010] easy-axis (c).

A square, exchange-biased M-H loop (H_{EB} = *60 Oe*; $J_K \approx 0.07$ *erg/cm²*, H_C = *90 Oe*), and a symmetric double-shifted loop, were observed for fields applied parallel to in-plane Fe[100] and [010] easy-axes, respectively. For fields applied in-plane along the Fe[110] minor hard-axis, exchange-bias is also observed, though the hard-axis response is retained, namely decreased remnant magnetization.

These results, along with vector magnetization measurements (shown later), our former Lorentz TEM observations[19], and comparison to magnetization measurements of an Fe layer (supplementary figure) show that the magnetization reversal along Fe easy-axes occurs through two successive steps: nucleation and propagation of 90° domain walls in which magnetic moments are aligned parallel to in-plane easy-axes of the Fe layer.

This reversal mechanism reflects a combination of unidirectional anisotropy aligned along the Fe[100] easy-axis direction, and Fe cubic magnetocrystalline anisotropy. The alignment of unidirectional anisotropy along the Fe[100] direction reflects coupling of Fe moments to the cubic antiferromagnetic structure of chemically-disordered γ-$IrMn_3$.

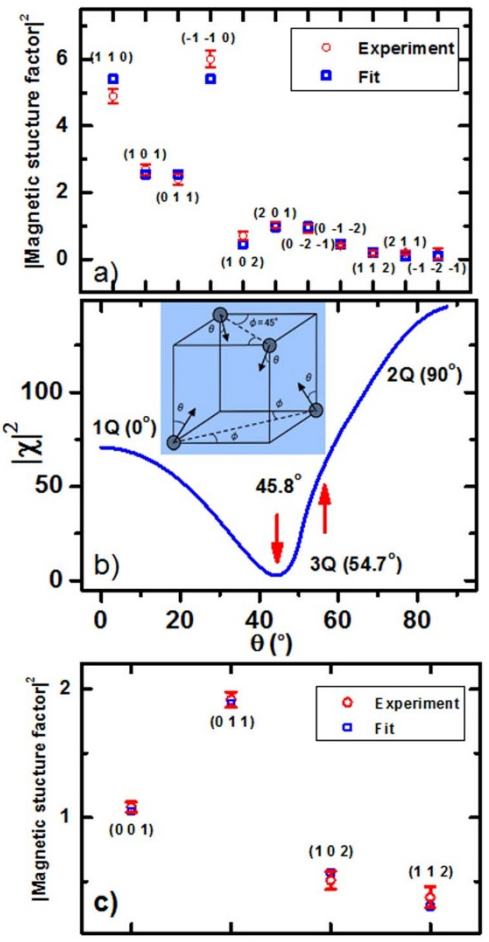

Figure 4 | Magnetic structure of $IrMn_3$ thin films. (a) Magnetic structure factors for all accessible reflections in chemically-disordered γ-$IrMn_3$. Calculated values of magnetic structure factors (blue points) are the best fit to observed intensities using the model shown in the inset of (b). (b) χ^2 goodness-of-fit test as a function of inter-spin angle, θ, defined in the inset. The inter-spin angle of 45° ± 2° represents a new magnetic structure of γ-$IrMn_3$ film (see Fig. 1b), ruling out 1Q(θ = 0°), 2Q(θ = 90°) and 3Q(θ = 54.7°) structures proposed for bulk γ-$IrMn_3$. (c) Magnetic structure factors for all accessible reflections in chemically-ordered $L1_2$-$IrMn_3$. Calculated values of magnetic structure factors (blue points) are the best fit to observed intensities using the T1 model (Fig 1a).

We note that comparable M-H loops were measured for a reverse bilayer epitaxial structure, namely BCC-Fe, MBE-grown on γ-$IrMn_3$ (identical layer thicknesses, see Fig. 4 supplementary). Hysteresis loops measured with a magnetic field applied along the direction of the unidirectional anisotropy axis, Fe[100], demonstrate the same reversal mechanism though H_{EB} is larger, *205 Oe*, and *Hc* lower, *60 Oe*, attributed to the deposition sequencing.

Additionally, the widths of 90° domain walls was measured in the exchange-biased Fe layer and compared to an Fe layer by using Fresnel-contrast defocused images in a Lorentz TEM. This width was estimated for Fe and exchange-biased Fe to chemically-disordered FCC $IrMn_3$ at 36 ± 6 nm and 32 ± 11 nm, respectively.

For interface-coupling of Fe moments to chemically-ordered $L1_2$-$IrMn_3$, magnetometry measurements show a significant increase of H_{EX} and H_C, *310 Oe* and *410 Oe*, respectively (Fig. 5d), namely $J_K \approx$ 0.37 erg/cm². More significant in this comparison between $L1_2$-$IrMn_3$

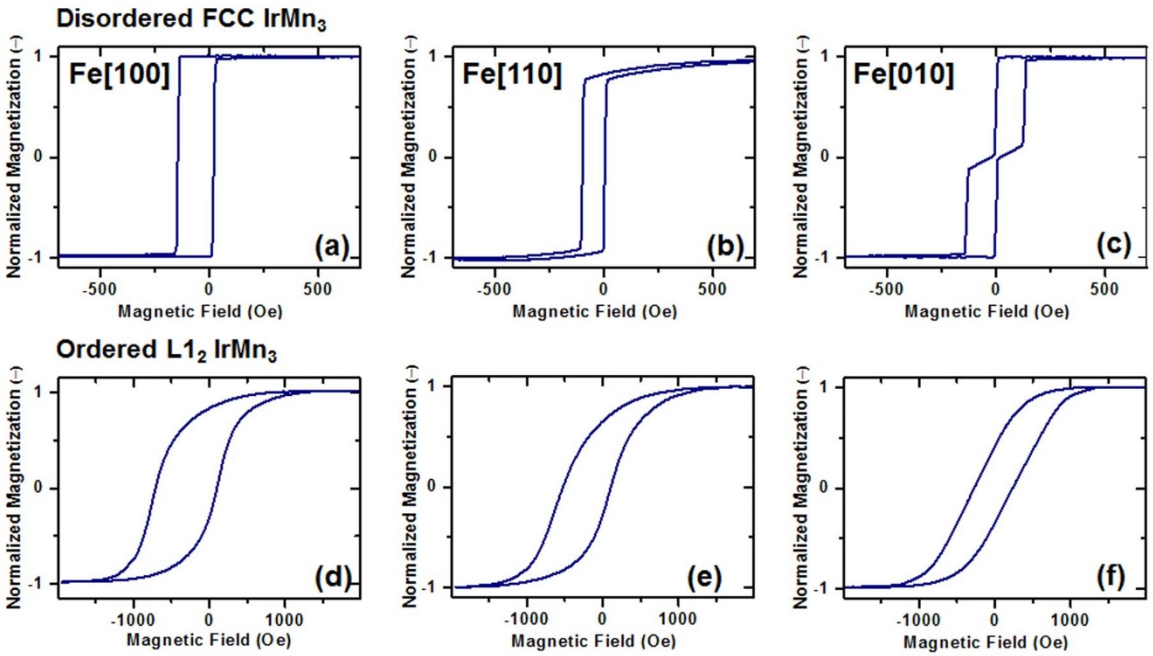

Figure 5 | Hysteresis loops for in-plane applied field, along Fe[100] easy-axis and magnetic-annealing direction(a,d), Fe[110] minor hard-axis direction(b,e), and Fe[010] second easy-axis direction(c,f), for chemically-disordered FCC $IrMn_3$(a–c) and chemically-ordered $L1_2$-$IrMn_3$(d–f).

and γ-$IrMn_3$, is that the reversal mechanism of Fe moments is now *rotational for all measured in-plane directions* of the applied field, as demonstrated in Fig. 5d–f, for in-plane Fe[100], Fe[010] easy-axes, and Fe[110] minor hard-axis direction, respectively. Lorentz TEM examination of this sample did not observe any domain walls.

To further understand the magnetization reversal process in Fe layers coupled to ordered $L1_2$-$IrMn_3$ and compare to the simpler reversal mechanism observed in Fe/γ-$IrMn_3$ bilayers, vector *M-H* measurements were undertaken, thus enabling to follow the 3-dimensional macroscopic transition of moments. These measurements (example shown in Fig. 6) show that coupling of the Fe magnetic moments to chemically-ordered $L1_2$-$IrMn_3$ indeed results in a rotational reversal process, which also includes an out-of-plane component. We note that detecting an out-of-plane magnetization component in soft Fe films (7 nm thick, $H_C \sim 10$ *Oe* before exchange-coupling, Fig.1supplementary) is highly irregular due to the strong demagnetization field. For chemically-disordered FCC-$IrMn_3$ layer, no out-of-plane magnetization component was detected in the Fe film. These observations, for Fe films coupled to γ-$IrMn_3$ or $L1_2$-$IrMn_3$ magnetic phases, were consistent for a wide range of directions of in-plane applied fields, and are demonstrated in the following example:

The magnetic field is applied in-plane along the Fe[010] easy-axis direction, which is perpendicular to the unidirectional anisotropy axis. Fig. *6a* shows measured magnetization components for γ-$IrMn_3$ along the [010] direction of applied field, and the [100] perpendicular direction, namely along the unidirectional anisotropy. No out-of-plane magnetization component ([001] direction) was detected within the 5 μemu sensitivity of the magnetometer, which is, as expected, due to the large demagnetizing field applied perpendicular to the surface of the Fe film. Vector *M-H* curves show that magnetization reversal indeed occurs through a two-stage process of nucleation and propagation of 90° domain walls as also verified by Lorentz TEM micromagnetic imaging. Vector measurements of the Fe/γ-$IrMn_3$ bilayer demonstrate alignment of unidirectional-anisotropy, whose origin we can attribute to the alignment of the cubic antiferromagnetic structure of γ-$IrMn_3$, with the Fe cubic magneto-crystalline anisotropy.

For chemically-ordered $L1_2$-$IrMn_3$, magnetization reversal is markedly different (Fig. 6b,c). In-plane components of magnetic moments follow a rotational process (Fig. 6b). Additionally, a small out-of-plane component (~5% of the saturation moment) is measured. As opposed to γ-$IrMn_3$, these results may be understood by the T1-triangular magnetic structure of $L1_2$-$IrMn_3$ antiferromagnet in which strong exchange-coupling between Mn moments enables an out-of-plane magnetization component of the Fe layer.

Discussion

The two crystallographic phases of $IrMn_3$ offer an opportunity to examine the influence of the antiferromagnetic structure on interface coupling to an epitaxial Fe ferromagnetic layer. Such a comparison is possible due to chemical order or disorder of $IrMn_3$, which results in two crystallographic cubic-symmetry phases with negligible differences in the lattice parameter and, important for this work, two very different antiferromagnetic structures. For chemically-ordered $L1_2$-$IrMn_3$ epitaxial thin films, we confirmed the T1 magnetic structure with three-fold symmetry that was previously reported for bulk $IrMn_3$. In the case of chemically-disordered γ-$IrMn_3$, we have solved the magnetic structure and report a new structure. The antiferromagnetic structure of γ-$IrMn_3$ epitaxial thin films is characterized by cubic-symmetry in which moments are tilted away by 45° from crystal diagonals towards the cube faces. We note that Fishman *et al.* reported for antiferromagnetic Ni_xMn_{1-x}*(x ~ 0.2)* alloys a similar structure[20]. Moreover, energy-calculations of Sakuma *et al.*, which predict that the 3Q structure of γ-$IrMn_3$ is most stable, show minor energy variations within a range of 10° around $\theta = 54.7°$. Those calculations are based on a cubic structure, for which the authors show that the angle of moments shifts slightly from 3Q towards 2Q when the lattice is distorted[13]. We observed in our γ-$IrMn_3$ films, an in-plane lattice expansion, which may cause this new magnetic structure to form. Expansive strain is common in thin metal films due to substrate clamping, thus we expect this new magnetic structure to be a general feature of epitaxial γ-$IrMn_3$ films.

Molecular beam epitaxial growth enabled to prepare exchange-biased bilayers of Fe/$IrMn_3$ in which the antiferromagnetic layer is

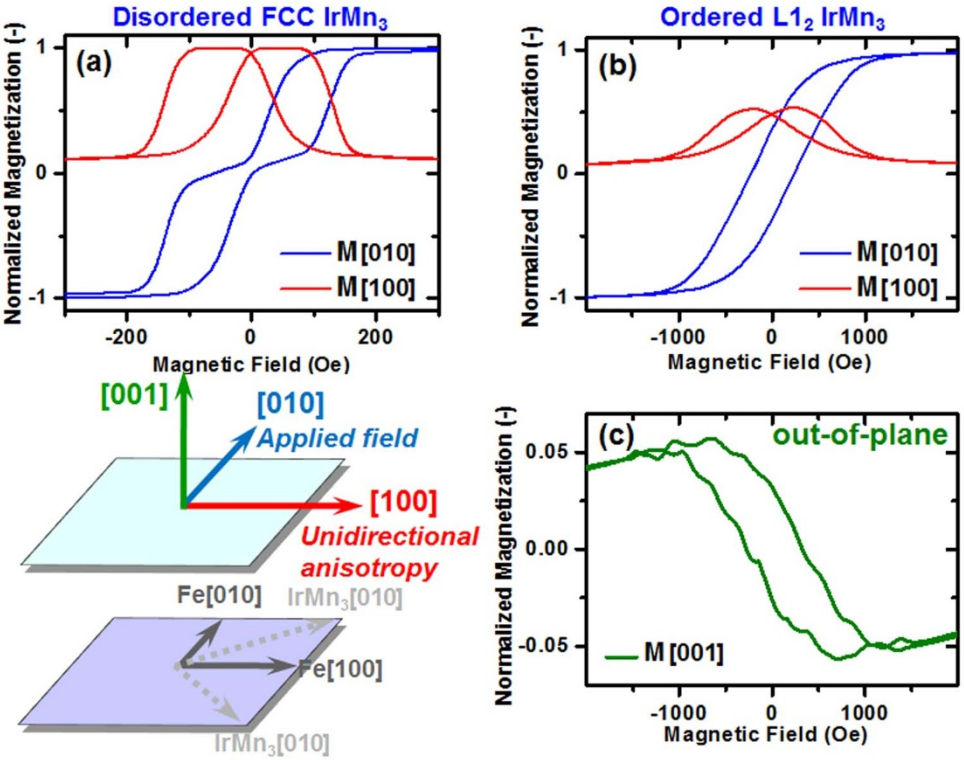

Figure 6 | Vector magnetization measurements when field is applied along Fe[010] direction (perpendicular to unidirectional anisotropy) for γ-$IrMn_3$(a) and $L1_2$-$IrMn_3$(b,c) Inset: top – schematic description of magnetization measurements with respect to crystallographic directions in the Fe layer; bottom – epitaxial relation between Fe and $IrMn_3$ for both bilayers.

controlled to be either chemically-disordered γ-$IrMn_3$ or chemically-ordered $L1_2$-$IrMn_3$. TEM and XRD analyses demonstrate the high structural quality and epitaxial similarity of these two bilayers, as well as sharp interfaces, and negligible chemical intermixing between the $IrMn_3$ and Fe layers.

Magnetometry of the two types of bilayers leads us to conclude that exchange-bias of the Fe layer is, in this case, determined to a large extent by the magnetic structure of the epitaxial $IrMn_3$ layer. For $L1_2$-ordering, the rotational magnetization reversal process and increased exchange-bias field is attributed to the triangular antiferromagnetic structure with strong coupling to Fe moments. The out-of-plane magnetization component can be attributed to a complex three-dimensional magnetic coupling at the interface. First-principles calculations[17] show that symmetry breaking at the $L1_2$-$IrMn_3$ interface results in large anisotropy effects, including perpendicular coupling of moments and substantial increase in unidirectional exchange-anisotropy. However, for FCC-$IrMn_3$, the cubic antiferromagnetic structure and weaker interface-coupling results in a reduced exchange-bias field of the Fe layer in which the reversal mechanism is initiated by 90° domain walls, which are aligned along BCC Fe easy-axes. The similarity of the widths of the 90° domain walls in the exchange-biased Fe film to an epitaxial Fe film indicates that unidirectional anisotropy does not influence significantly the structure of the domain wall. Therefore, exchange-bias acts to pin the magnetic moments of the Fe layer at the interface, but does not appear to change its intrinsic magnetic properties.

Methods

Molecular Beam Epitaxy growth of exchange-biased layers. The magnetic thin layers were deposited in ultra-high vacuum (UHV) conditions by molecular beam epitaxy on single crystalline, MgO(001) substrates, sized 10×12 mm^2. The substrates were annealed at 700°C for 30 minutes in UHV conditions. A 20-nm-thick MgO buffer layer was deposited at 500°C prior to the deposition of the magnetic layers. For the disordered $IrMn_3$ sample, 7 nm of Fe followed by 15 nm of $IrMn_3$ layers were deposited in the presence of a magnetic field of 150 Oe along the Fe[100] direction. The Fe layer was deposited at 200°C and annealed at 400°C for 30 minutes before the $IrMn_3$ layer was deposited at room temperature and then capped with a 10-nm-thick Cr layer.

Comparable reverse-sequence samples were prepared in which the BCC Fe was grown on top of chemically-disordered γ-$IrMn_3$ (identical thicknesses of the layers). The substrate temperature was kept low, at 100 °C, thus resulting in a chemically-disordered $IrMn_3$ layer. This bilayer was capped with a 10 nm thick Ir layer.

The ordered $L1_2$-$IrMn_3$ layer was deposited on a 30-nm-thick Ir buffer layer at 400°C and followed by deposition of a 7 nm thick Fe layer, and capped with a 10-nm-thick Cr layer.

The stoichiometric composition of the various $IrMn_3$ layers was verified by wavelength dispersive X-ray spectroscopy in a scanning electron microscope and energy-dispersive spectroscopy in STEM. Additional information on the development of the growth methodology of epitaxial FCC-Ir_xMn_{1-x} layers is presented in Ref. 19.

Structural characterization. The microstructure of the samples was examined using several TEM-related methodologies with a JEOL 2200MCO image- and probe aberration adjusted microscope equipped with an Ω-type electron energy filter.

Cross-sectional TEM samples were prepared by tripod mechanical polishing and Ar ion-milling using a Gatan Precision Ion Polishing System and Fischione model 1010 ion miller.

For HRTEM (phase-contrast) observations, which are presented here as the raw recorded data, a negative spherical aberration coefficient was chosen, between −5 and −10 μm. To characterize the interface structure, the spherical-aberration of the objective lens was adjusted to these values in order to reduce significantly spatial delocalization, and so that the measured intensity at locations of atomic columns is larger, namely appear bright. The HRTEM multi-slice image simulation of the interface structure was performed using the CrystalKit and JEMS programs[21].

Energy-filtered TEM spectrum imaging was applied for chemical mapping with convergence and collection angles of 6 and 24 mrad, respectively. The thickness of the samples was measured with a zero-loss image using a 5 eV energy slit width. Typical sample thicknesses of under 0.7 of the electron mean-free-path were measured, which enables quantitative analysis. Both core-loss and low-loss mapping were applied for compositional mapping of the layers. For all spectrum image data sets, the spatial drift between images was corrected by an algorithm developed by Schaffer *et al.*[22].

Core-loss spectrum image data was used to calculate areal density maps. Low energy-loss mapping was performed using multiple linear least-squares (MLLS) fitting of typical spectra of the various layers. For both approaches, scripts developed by Gatan for Digital Micrograph 3.10 were applied.

Low-loss energy data series were collected between 10 and 100 eV with an energy slit width of 5 eV. The energy step size was 2 eV with an exposure time of 5 seconds.

Results of this data analysis are presented in Fig. 2a with the following colour representations: MLLS fit to typical low-loss spectra in the Fe (red), $IrMn_3$ (green) and Cr (blue) layers.

The core-loss series was collected between 450 and 800 eV with an energy slit width of 20 eV. The energy step size was 10 eV with an exposure time of 30 seconds. Within that energy range, the following core edges were quantified for mapping: O K 532 eV, Cr L_3 575 eV, Mn L_3 640 eV, Fe L_3 708 eV. The results of this fitting are shown in Fig. 2b with the following colour representations: Fe L (red), Mn L (green) and Cr L (blue).

For HAADF STEM imaging, the probe convergence semi-angle was 16 mrad and camera length was 50 mm, giving a collection inner semi angle of 50 mrad and an outer semi-angle of 140 mrad. The spatial resolution is approximately 0.1 nm. A Butterworth filter, using a fraction of 0.5, was applied to the HAADF-STEM images to improve the image quality[23].

Lorentz microscopy was performed to image the micro-magnetic structure of the Fe/IrMn bilayers using a JEOL 4000EX side-entry TEM (LaB_6 filament) fitted with a low-field objective pole-piece. An in-plane magnetic field spanning the range $\pm$400 Oe was applied *in situ* in the microscope, along different in-plane angles, using coils mounted on the sample holder. Due to the epitaxial growth on MgO, the TEM samples were prepared by a conventional grinding method followed by thinning to electron transparency using Ar ion milling. The samples were prepared so that a large field of view in the TEM was achieved (approximately 30 μm in diameter). In addition, ion milling was stopped before a hole was formed in the sample in order to prevent artifacts in the magnetic structure.

The widths of the 90° domain walls in the exchange-biased Fe layer and Fe layer was estimated by using Fresnel-contrast defocused images in a Lorentz TEM. The full-width half-maximum (FWHM) of the image intensity perpendicular to divergent 90° domain walls was measured as a function of the defocus distance. The width of the domain wall is estimated by extrapolating the measured FWHM results to zero defocus[24,25].

X-ray diffraction data were collected using a Siemens D5000 X-Ray diffractometer with an incident wavelength of 1.54Å. The chemical ordering parameter (S) of the $IrMn_3$ layer was determined using the integrated intensity ratio of the $IrMn_3$ (001)/(002) and (003)/(004). Detailed calculation procedures for measuring S can be found in Ref. 26. The mosaic spread was found by rotating the sample about an axis perpendicular to the scattering plane.

The in-plane lattice constant of γ-$IrMn_3$ was determined from the $IrMn_3$(022) reflection. The in-plane lattice constant of $L1_2$-$IrMn_3$ was determined from (011) and (022) reflections.

Magnetic structure and Macro-magnetic properties. The magnetic structure of the $IrMn_3$ film was investigated by neutron diffraction using the D10 diffractometer at ILL France in four-circle mode with a wavelength of 2.36Å and a crystal analyser between the sample and detector set to zero energy transfer to reduce the inelastic background. The samples were grown using a similar protocol as described before. The $IrMn_3$ layers were thicker in this case, 200 nm thick, in order to improve the accuracy of the measurement. Chemically-disordered γ-$IrMn_3$ and chemically-ordered $L1_2$-$IrMn_3$ layers were achieved by growing at room temperature and 700 °C, respectively. The layers were capped with a 10 nm thick Ir layer.

The macro-magnetic properties of the samples were measured using a Lakeshore VSM, while vector VSM measurements were undertaken using a MicroSense system.

1. Meiklejohn, W. H. & Bean, C. P. New magnetic anisotropy. *Phys. Rev.* **102**, 1413–1414 (1957).
2. Nogués, J. & Schuller, I. K. Exchange bias. *J. Magn. Magn. Mater.* **192**, 203 (1999).
3. Berkowitz, A. E. & Takano, K. Exchange anisotropy - a review. *J. Magn. Magn. Mater.* **200**, 552–570 (1999).
4. Nogués, J. *et al*. Exchange bias in nanostructures. *Physics Reports* **422**, 65–117 (2005).
5. Radu, F. & Zabel, H. 2008 Exchange bias effect of ferro-/antiferromagnetic heterostructures *Magnetic Heterostructures* (*Springer Tracts in Modern Physics* vol. 227) (Berlin: Springer) p. 97–184.
6. Chappert, C., Fert, A. & Nguyen Van Dau, F. The emergence of spin electronics in data storage. *Nature Materials* **6**, 813–823 (2007).
7. Kuch, W. *et al*. Tuning the magnetic coupling across ultrathin antiferromagnetic films by controlling atomic-scale roughness. *Nature Materials* **5**, 128–133 (2006).
8. Ali, M., Marrows, C. H. & Hickey, B. J. Controlled enhancement or suppression of exchange biasing using impurity δ layers. *Phys. Rev. B* **77**, 134401 (1–7) (2008).
9. Morales, R. *et al.* Role of the antiferromagnetic bulk spin structure on exchange bias, *Phys. Rev. Lett.* **102**, 097201 (2009).
10. Yamaoka, T. Antiferromagnetism in γ-phase Mn-Ir alloys. *J. Phys. Soc.* Japan, **36**, 445–450 (1974).
11. Devasahayam, A. J. & Kryder, M. H. Biasing materials for spin-valve read heads. *IEEE Trans. Magnet.* **35**, 649 (1999).
12. Yamaoka, T., Mekata, M. & Takaki, H. Neutron diffraction study of γ-phase Mn-Ir single crystals. *J. Phys. Soc. Japan*, **36**, 438–444 (1974).
13. Sakuma, A., Fukamichi, K., Sasao, K. & Umetsu, R. Y. First-principles study of the magnetic structures of ordered and disordered Mn-Ir alloys. *Phys. Rev. B* **67**, 024420(1–7) (2003).
14. Tomeno, I., Fuke, H. N., Iwasaki, H., Sahashi, M. & Tsunoda, Y. Magnetic neutron scattering study of ordered Mn_3Ir. *J. Appl. Phys.* **86**, 3853–3856 (1999).
15. Szunyogh, L., Lazarovits, B., Udvardi, L., Jackson, J. & Nowak, U. Giant magnetic anisotropy of the bulk antiferromagnets IrMn and $IrMn_3$ from first principles. *Phys. Rev. B* **79**, 020403(R)(1–4) (2009).
16. Tsunoda, M., Imakita, K., Naka, M. & Takahashi, M. $L1_2$ phase formation and giant exchange anisotropy in Mn_3Ir/Co-Fe bilayers. *J. Magn. Magn. Mat.* **304**, 55–59 (2006).
17. Szunyogh, L., Udvardi, L., Jackson, J., Nowak, U. & Chantrell, R. Atomistic spin model based on a spin-cluster expansion technique: Application to the $IrMn_3$/Co interface. *Phys. Rev. B* **83**, 024401(1–9) (2011).
18. Umebayashi, H. & Ishikawa, Y. Antiferromagnetism of γ Fe-Mn alloys. *J. Phys. Soc.* Japan, **21**, 1281–1294 (1966).
19. Wang, S. G. *et al*. Exchange bias in epitaxial $Fe/Ir_{0.2}Mn_{0.8}$ bilayers grown on MgO (001). *J. Phys. D: Appl. Phys.* **42**, 225001(1–8) (2009).
20. Fishman, R. S. *et al*. Structural and magnetic phase transitions in Mn-Ni alloys. *Phys. Rev. B* **61**, 12159–12167 (2000).
21. Stadelmann, P. A. EMS - a software package for electron diffraction analysis and HREM image simulation in materials science. *Ultramicroscopy* **21**, 131–146 (1987).
22. Schaffer, B., Grogger, W. & Kothleitner, G. Automated spatial drift correction for EFTEM image series. *Ultramicroscopy* **102**(1), 27–36 (2004).
23. Russ, J. C. in '*The Image Processing Handbook*', CRC Press, Taylor and Francis Group (2007).
24. Gong, H. & Chapman, J. N. On the use of divergent wall images in the Fresnel mode of Lorentz microscopy for the measurement of the width of very narrow domain-walls. *J. Magn. Magn. Mat.* **67**(1), 4–8 (1987).
25. McVitie, S. & Cushley, M. Quantitative Fresnel Lorentz Microscopy and the transport of intensity equation. *Ultramicroscopy* **106**(4–5), 423–431 (2006).
26. Imakita, K., Tsunoda, M. & Takahashi, M. Thickness dependence of exchange anisotropy of polycrystalline Mn_3Ir/Co-Fe bilayers. *J. Appl. Phys.* **97**, 10K106 (1–3) (2005).

Acknowledgements

We are grateful to Mr. Keith Belcher for technical support, to the Institut Laue-Langevin for the allocation of neutron beam time, and to the Engineering and Physical Sciences Research Council (EPSRC UK) for funding this research project. We thank Dr Erik Samwell for assistance with vector magnetometry.

Author contributions

A.K. (corresponding author) and R.C.C.W. planned the experiment. R.C.C.W. grew the epitaxial samples. A.K. and A.K. carried out the TEM and magnetometry measurements and the subsequent structural and magnetic properties characterization. J.P.G., R.F. and R.C.C.W. carried out X-ray diffraction measurements and the subsequent structural analysis. J.P.G., R.F. and G. J. M. carried out neutron scattering measurements and the subsequent magnetic structure analysis. All the co-authors contributed to the analysis and discussion for the results. A.K. and A.K. wrote the main body of the text with all co-authors contributing with their respective growth, measurements and characterization as well as an overall contribution to the manuscript.

Additional information

Supplementary information accompanies this paper at http://www.nature.com/scientificreports

Competing financial interests: The authors declare no competing financial interests.

How to cite this article: Kohn, A. *et al.* The antiferromagnetic structures of $IrMn_3$ and their influence on exchange-bias. *Sci. Rep.* **3**, 2412; DOI:10.1038/srep02412 (2013).